Photonic Generation of 30 GHz Bandwidth Stepped-Frequency Signals for Radar Applications

Ziqian Zhang, *Student Member, OSA*, Yang Liu, *Member, OSA*, and Benjamin J. Eggleton, *Fellow, IEEE*

***Abstract*—Wideband microwave signals with high time-frequency linearity for high-resolution radar applications can be optically generated using high-speed electronic waveform generators. Frequency-shifting modulation in an optical cavity provides an attractive approach to generate broadband microwave signals with reduced complexity requiring only MHz-level electronics. However, the in-loop signal instability and inter-pulse interference usually cause amplitude fluctuations, leading to limited signal-to-noise ratio and signal bandwidth. Here, we overcome these challenges and demonstrate, for the first time, the photonic generation of 30-GHz-wide stepped-frequency (SF) signals with 100 MHz frequency steps defined by an MHz-level electrical oscillator. We achieved this performance by mitigating the in-loop polarization scrambling and inter-pulse interference using a polarization-maintaining cavity and a high-extinction optical switch. This allows stable consecutive acousto-optic frequency-shifting modulation that significantly improves the signal-to-noise ratio. While achieving a bandwidth surpassing the state-of-the-art demonstrations based on wideband electronics, our approach alleviates the necessity for high-speed signal generators or wideband tunable lasers. To exemplify the utility, we systematically evaluate the signal quality and show its applications in radar imaging compared to those using electrical waveform generators.**

***Index Terms*—Microwave photonics, photonic radar, synthetic aperture radar, ultra wideband radar.**

I. Introduction

RADAR sensing has been progressing into the millimeter-wave (MMW, 30-300 GHz) and terahertz-wave (THz-wave, 0.1-10 THz) regions to operate with ultra-wide bandwidths for growing demands of high spatial resolution imaging in real-world applications, such as non-destructive testing, automotive driving assistance, industrial quality inspection, and non-invasive medical imaging [1]–[5]. However, the development of wideband radars operated at high frequencies has posed challenges to conventional electronic technologies, especially in synthesizing ultra-broadband signals. Multi-stage frequency up-conversion could lead to degradations in both efficiency and noise level when approaching higher frequencies [6]. Additionally, frequency multiplexing and spectrum stitching for bandwidth broadening introduce noise and spectrum spurs induced by device nonlinearity and interference [7] that compromises overall sensing accuracy and performance.

Microwave photonics has shown significant advantages in radio-frequency (RF) signal generation, up-conversion [8]–[12], and demodulation [7], [13]–[15], enabling flexible tunability of signal bandwidth and operation frequency [16]–[22]. Ultra-wideband linear-frequency modulated (LFM) signals that are widely adopted for radar and sensing applications can be optically synthesized [23]–[30]. Existing photonic approaches for LFM generation usually rely on high-speed benchtop electronics or elaborately biased electro-optic modulators (EOMs), which have limited bandwidth constrained by the electronics speed and long-term operational stability caused by EOMs' bias-drifting [28], [31]. Approaches using dispersion-based time-stretch [32] and frequency-sweeping light sources [26], [33], [34] have also shown promising bandwidth capacity but require elaborate pre-distorted RF control signals for linearity compensation.

Another widely-used signal format in radars relies on stepped-frequency (SF) waveforms that can exhibit high time-frequency linearity and small spontaneous processing bandwidth while sustaining the same range resolution for the same bandwidth with the LFM signals [35]. Photonic generation of SF signal using frequency shifting modulation has been recently demonstrated [36]–[39], showing advantages of bandwidth flexibly while sustaining a high time-frequency linearity in radar ranging and imaging system demonstrations. In principle, the SF signal bandwidth can be adjusted by tuning the passband of an optical filter [37], [39], modifying the RF frequency applied to the EOM [38], and electronically controlled in-loop switch [40]. However, in practical implementations, achieving an ultra-wide bandwidth of $>$20 GHz with an MHz-level frequency step required for an extended unambiguous range is challenging due to the loop instability, particularly after a large number of re-circulations. This usually results in an increased signal amplitude fluctuation and low SNR, limiting the achievable bandwidth of the system. Moreover, the SF radar signal quality and performance have not been explored in comparison with conventional photonic radar schemes.

Manuscript received January 24, 2022; revised March 4, 2022; accepted March 31, 2022. Date of publication April 4, 2022; date of current version July 16, 2022. This work was supported in part by the U.S. Air Force (USAF) under Grant FA2386-16-14036, in part by the U.S. Office of Naval Research Global (ONRG) under Grant N62909-18-1-2013, and in part by Australian Research Council Discovery Project under Grant DP-200101893. *(Corresponding Author: Yang Liu.)*

The authors are with the University of Sydney Nano Institute (Sydney Nano), Institute of Photonics and Optical Science (IPOS), School of Physics, The University of Sydney, Sydney, NSW 2006, Australia (e-mail: ziqian.zhang@sydney.edu.au; yang.liu@sydney.edu.au; benjamin.eggleton@sydney.edu.au).

Color versions of one or more figures in this article are available at https://doi.org/10.1109/JLT.2022.3164637.

Digital Object Identifier 10.1109/JLT.2022.3164637

In this work, we extend on our previous demonstration by overcoming the frequency-shifting loop instability and demonstrate, for the first time, an SF signal with tunable bandwidth reaching 30 GHz using MHz-level electronics-enabled photonic signal synthesis. Our approach takes advantage of a polarization-maintaining optical cavity, which is robust against the ambient environment perturbation and free from modulation bias drifting. As a result, the demonstrated approach reaches a signal-to-noise ratio (SNR) of above 34 dB in the signal generation on par with those generated by high-end benchtop electronics. We apply the signal generation scheme to an inverse synthetic radar (ISAR) system and experimentally compare the imaging performance with photonic radars using a high-speed waveform generator, demonstrating its viable utilities in applications. With the achieved bandwidth and potential for further extension, this demonstrated approach provides a complementary approach for ultra-wideband microwave waveform synthesis in MMW and THz-wave radar systems.

II. Principle

The SF waveforms are generated through recirculating a rectangular optical pulse signal in a frequency-shifting loop (FSL) [36], [37], [41], as diagrammed in Fig. 1(a). An optical switch (OS) converts a continuous wave (CW) laser signal into an initial rectangular optical pulse signal for further frequency shifting in the loop. An acousto-optic modulator (AOM) precisely shifts the pulse frequency for each round-trip, synthesizing a bandwidth of B after N-time recirculations (N steps) with a constant MHz-level frequency shift Δf, as illustrated in Fig. 1(b). The high-extinction, bias-free AOM-based frequency shifting avoids the generation of spectral harmonic spurs, which is an outstanding advantage over the approach using EOMs for single-sideband modulation (SSB) that suffers from bias drifting and parasitic harmonics [31], [38]. An erbium-doped fiber amplifier (EDFA) is used to compensate for the optical modulation and couplers losses. The constant ratio between the frequency shift (Δf) and the loop round trip time ensures the time-frequency linearity of the synthesized SF waveform for accurate detections. In the proof-of-concept demonstrations, a tunable optical bandpass filter (OBPF) is used to determine the bandwidth of the generated microwave SF signal and filter out the out-of-band amplifier's noise. Consequently, the time-domain waveform is a series of sub-pulses with the sub-pulses frequency discretely hopping at a spacing of the AOM's RF driving frequency Δf, as illustrated in Fig. 1(c) and (d). Microwave up-conversion to high frequencies is achieved by mixing the SF signal with a frequency-shifted CW laser in photodetection.

As shown in Fig. 1(c), one general challenge of achieving broadband and stable microwave photonic SF signals is the instability of the circulating optical signals in the loop, which indeed leads to amplitude fluctuations and thus the single-pass optical gain in the loop. The amplitude variations could equally result in transient gain suppression and increased noises due to the gain dynamics in the EDFA, leading to a limited circulating number and ultimately the achievable bandwidth. In order to overcome this issue, a polarization-maintained optical cavity

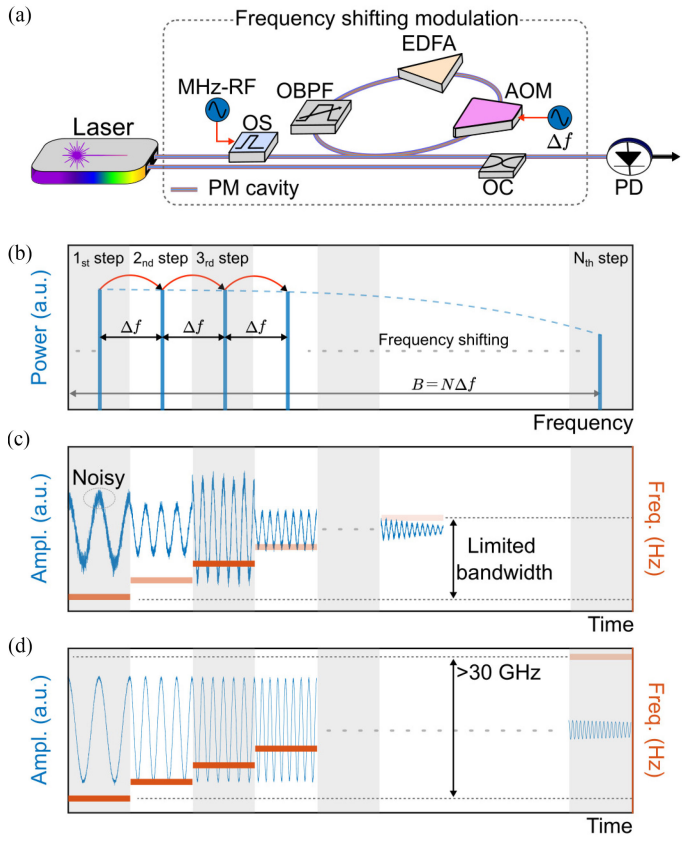

Fig. 1. Principle of stepped frequency (SF) signal generation with improved bandwidth and signal-to-noise ratio (SNR). (a) Schematic of the demonstrated SF signal generation using optical frequency-shifting modulation based on the polarization-maintaining (PM) cavity for radar applications. (b) Principle of the SF signal generation using optical frequency-shifting modulation on the frequency domain. The signal's frequency will be shifted by Δf for each recirculation time in the cavity, thus synthesizing a total bandwidth $BW = N\Delta f$. Schematic illustrations of generated stepped-frequency waveforms based on (c) an unoptimized frequency-shifting loop using a low-extinction ratio optical switch ($\sim$20 dB) and single-mode fiber components, and (d) an optimized loop using a high-extinction ratio optical switch ($>$40 dB) and polarization-maintaining components to suppress the amplitude fluctuations caused by polarization scrambling, respectively. RF, radio-frequency; OS, optical switch; OBPF, optical bandpass filter; EDFA, erbium-doped fiber amplifier; AOM, acousto-optic modulator; OC, optical coupler; PD, photodetector.

is implemented to mitigate the signal polarization scrambling. In Fig. 1(d), with stabilized polarization and the robustness against ambient perturbations, broader bandwidth SF signals with reduced amplitude fluctuations and noises can be synthesized. These approaches can significantly improve the SNR and effectively increase the achievable bandwidth for higher spatial resolution [35], [42].

A high-quality signal with a broad bandwidth and less noise is highly desirable when deploying SF signals for various applications to ensure high resolution and accuracy. In principle, the demonstrated system can achieve arbitrary bandwidth tuning by changing the passband and central frequency of the OBPF, thereby enabling range resolutions down to millimeter level. However, in practice, such broadband synthesizing is challenging for single-mode fibers (SMFs) since the signal's polarization state is scrambled in the optical cavity, which deteriorates the

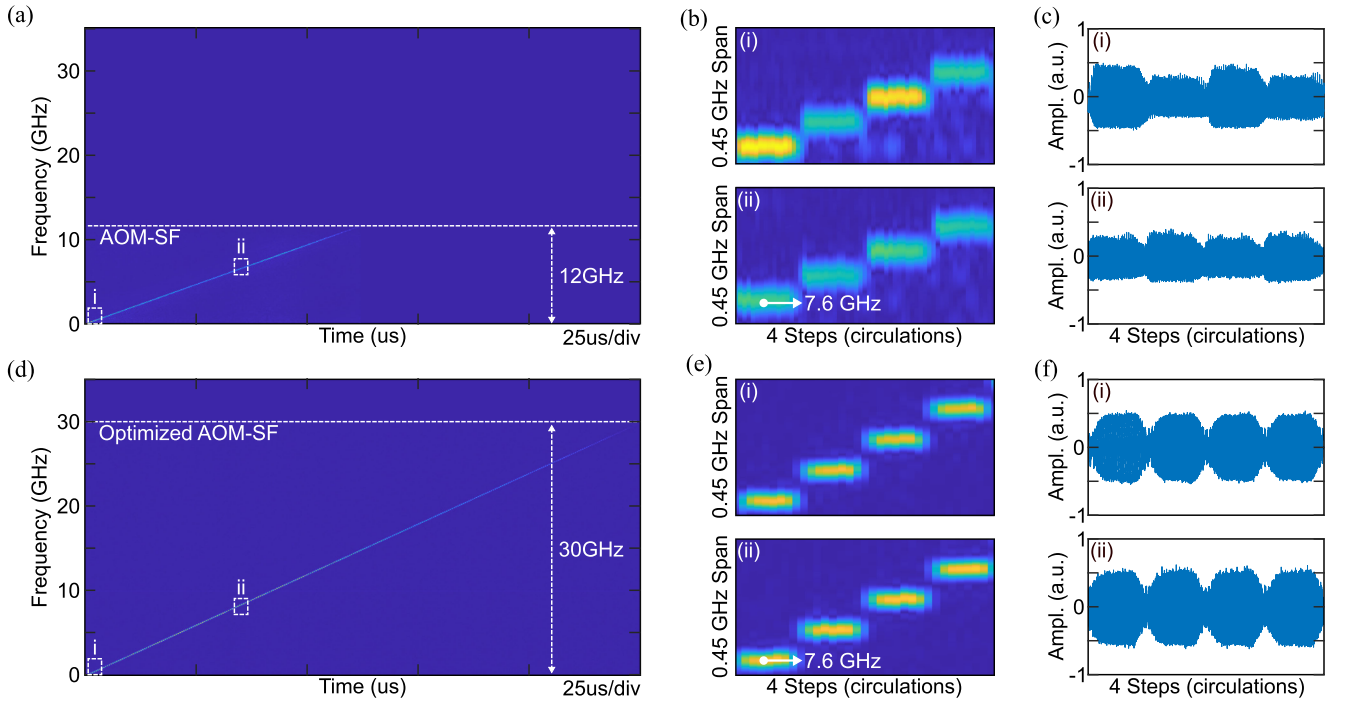

Fig. 2. Comparisons of the maximum achievable bandwidth and signal quality between SF generators with and without polarization stabilization. (a) Time-frequency analysis of the signal generated through an un-optimized FSL using SMFs with a bandwidth of 12 GHz. (b) Two insights of the 12-GHz SF signal showing: (i) the first four frequency steps and (ii) four frequency steps with a starting frequency of 7.6 GHz, in the time-frequency domain. (c) The corresponding time-domain waveforms of the 12-GHz insights. (d) Time-frequency analysis of the signal generated through an optimized FSL using PMFs with a bandwidth exceeding 30 GHz. (e) Two insights of the 30-GHz SF signal showing: (i) the first four frequency steps and (ii) four frequency steps with a starting frequency of 7.6 GHz, in the time-frequency domain. (f) The corresponding time-domain waveforms of the 30-GHz insights.

phase stability, signal coherence, and ultimately the sensing performance. As shown in Fig. 2(a), the time-frequency plot of the SF signal generated through an FSL using SMFs is struggled to achieve a bandwidth of 12 GHz. Fig. 2(b) provides insights into the time-frequency domain with the corresponding time-domain waveforms plotted in Fig. 2(c), revealing the amplitude fluctuations across different frequency steps, caused by the polarization and gain instabilities. These instabilities degrade the signal's quality, specifically the SNR, thus deteriorating the radar's performance, such as the maximum detection range and ranging accuracy [35], [43].

In contrast, the signal bandwidth and stability can be significantly increased using polarization-maintaining fibers (PMFs) and components that can minimize the polarization scrambling and suppress the polarization-dependent amplified spontaneous emission (ASE) noise from the EDFA [36]. This improvement allows achieving the ultra-broad bandwidth synthesizing over 30 GHz, as shown in Fig. 2(d). In addition, using a high on-off extinction ratio OS (from ∼20 dB to >40 dB extinction ratio) can suppress the seed pulse tails recirculating in the FSL. Therefore, the background noise and amplitude fluctuation in Fig. 2(e) is significantly reduced compared with Fig. 2(b). As a result, Fig. 2(f) shows that the system generates a more stable pulse-circulation with a significant reduction in amplitude noises.

To provide more insights into the signal quality, we compare the SNR of the signal generated using different schemes. Fig. 3(a) shows the SNRs of the SMF-based system with a synthesized bandwidth of 12 GHz at two specific step numbers, i.e., 10-time (blue) and 60-time (red) recirculation, revealing an SNR of 17.75 dB. In contrast, Fig. 3(b) shows a minimum SNR of 34.10 dB at 60-time (red) recirculation of a 25 GHz bandwidth SF signal using a PMF-based loop, providing a 14 dB SNR improvement. Importantly, even after 200-time recirculation (yellow), the optimized system exhibits only a 2.2 dB degradation, as shown in Fig. 3(b). An SNR analysis for the scheme based on an arbitrary waveform generator (AWG, Keysight M8195A 65GSa/s, 25 GHz analog bandwidth) is shown in Fig. 3(c) to benchmark the performance. It shows that the demonstrated system sustains an SNR above 34 dB after 60-time recirculation in the PMF-based FSL compared with 39 dB SNR from the high-end electronics in Fig. 3(c). The results indicate that the demonstrated PM-based system could achieve a similar SNR performance with those high-speed electronic synthesizers, while it eliminates the necessity of using wideband AWGs for SF signal generation. In the above analysis, waveform clips with a time window of 25 ns are extracted at specific step numbers (times of recirculation) for Fourier analysis.

In order to demonstrate the competitive performance and utility, we compare radar imaging results based on the demonstrated SF signal generator with those using high-speed electronic AWGs, as shown in Fig. 4(a). 2D imaging experiments are conducted based on the ISAR technique [43], i.e., stacking multiple ranging results to extract 2D images of a moving target, as shown in Fig. 4(b). The experiment also compares the SF waveform with the LFM waveform as a performance benchmark.

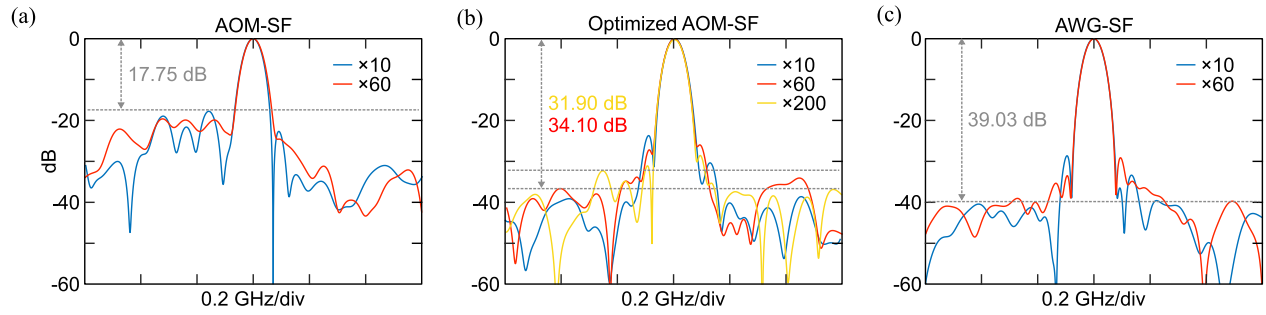

Fig. 3. Signal-to-noise ratio (SNR) comparisons among the system based on SMFs, PMFs, and an arbitrary waveform generator (AWG) with a sampling rate of 65 GSa/s (~25 GHz analog bandwidth). (a) SNR plots of the SMF-based system at two frequency instances, i.e., 10-time recirculation (blue) and 60-time recirculation (red) with SNRs around 17.75 dB. The signal has a bandwidth of ~12 GHz. (b) SNR plots of the PMF-based system at the same frequency instances showing an SNR of 34.10 dB at 60-time recirculation. Moreover, 200-time recirculation is plotted (yellow) with an SNR of 31.90 dB. The signal has a bandwidth of ~25 GHz to match with the analog bandwidth of the AWG. (c) SNRs of the SF signal generated using an AWG at the same frequency instances. The SNR results are calculated using 25 ns time-domain clips.

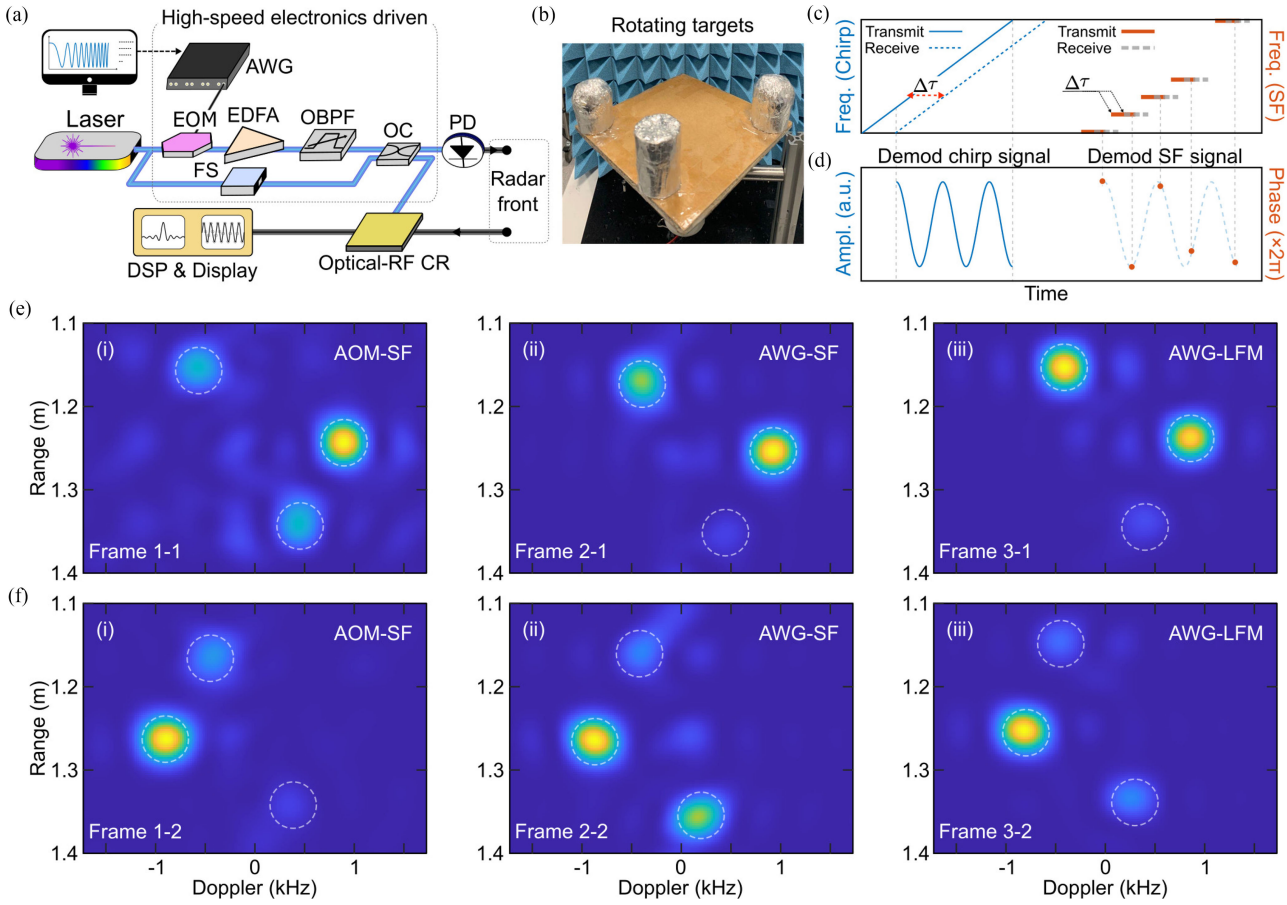

Fig. 4. Experimental results of the demonstrated system showing a comparable 2D imaging performance to an AWG-enabled photonic radar using both stepped-frequency (SF) and linear-frequency modulated (LFM) signals. (a) Schematic of a photonic radar system driven by a high-speed signal generator, which compares the imaging performance with the proposed radar system. (b) The target for radar imaging with three-cylinder objects mounted on a rotating platform. (c) Principal comparisons of radar systems using LFM and SF signals. (d) Demodulated LFM and SF signals in a radar receiver. (e, f) 2D imaging results. EOM, electro-optic modulator; AWG, arbitrary waveform generator; FS, optical frequency shifter; PD, photodetector; DSP, digital signal processing; CR, coherent receiver.

Fig. 4(c) shows the principle of the SF signal, in comparison to LFM signals, which are both widely used as pulse-compression waveforms for radar sensing, owing to their benefits of higher mean powers while sustaining superior resolution [43]. The operation principles of the SF signal and the LFM signal have fundamental but subtle differences; intuitively, the SF signal is a discretely sampled version of the LFM signal, as shown in Fig. 4(d). In radar applications, the SF radar encodes the time

delay ($\Delta\tau$) of the reflected signal as phase differences with respect to the reference signals

$$\omega_{SF} \propto 2\pi n \Delta f \Delta\tau, \tag{1}$$

where Δf is the incremental frequency, and $n = 1, \ldots, N$, N is the total number of frequency steps [43]. The LFM radar forms a new oscillating angular frequency at the receiver, proportional to the round-trip time $\Delta\tau$, which can be expressed as

$$\omega_{LFM} \propto 2\pi k \Delta\tau t, \tag{2}$$

where $k = bw/T$ is the chirp rate, bw is the signal's bandwidth, and $1/T$ is the repetition rate of the wideband signal [44].

For comparison, we implement AWG-based radar systems with the same bandwidth ($\sim$5.76 GHz), repetition rate (25 us), and RF radiation power ($\sim$10 dBm). The signal bandwidth in the demonstration was chosen due to the bandwidth availability of the RF antennas and the RF amplifiers but without losing generality for performance comparison. Wideband-RF signals generated by the AWG modulate a CW laser carrier through an electro-optic single-sideband modulation before beating with a separate optical carrier for optical-RF up-conversion. As shown in Fig. 4(b), three-cylinder objects mounted on a rotating platform (at a speed of $\sim$30 rad/s) are used as the target. Each ISAR image shown in Fig. 4(e) and (f) used 100 continuou ranging results (2.5 ms in total) to extract the Doppler information. Imaging results in Fig. 4(e) and (f) are chosen at two particular instances for an adequate performance illustration and comparison, proving that the demonstrated system is reliable for imaging moving objects. It is worth mentioning that the rotational motion of the object mainly causes the speckle-like noise on the images' background, which can be mitigated using motion compensation algorithms [35], [43]. Notably, the demonstrated system successfully reconstructed ISAR images of the objects without distinguishable differences from the SF- and LFM-based radars driven by the wideband AWG.

III. Discussion

The SF waveforms have shown several advantages over the LFM signals. For instance, it possesses an increased dynamic range due to each frequency step's narrow instantaneous noise bandwidth for signal processing while preserving the range resolution, and the overall bandwidth [4]. However, the SF waveform has a smaller unambiguous range defined by $c/2\Delta f$, where c is the propagation speed of the RF signal in the air. The 100 MHz frequency shift in the demonstrated system has a theoretically unambiguous range of 1.5 meters. This limitation can be feasibly overcome by using a minor frequency step (Δf). One way of achieving the minor frequency step is to cascade two AOMs with the opposite frequency shift (e.g., a frequency shift from -10 to +10 MHz has been demonstrated in [45]) to achieve an unambiguous range over 100 meters, comparable to the 120 meters unambiguous range window (1.25 MHz frequency shift) from the CARABAS system – a very early airborne synthetic aperture radar that employed SF signals — mounted on an aircraft [46]. It should be noted that the radar's maximum detection range is not limited by its unambiguous range [35], [47]. In the demonstrated system, long-range detection can be realized similarly to the CARABAS, i.e., introducing a variable time delay to the reference SF signal, setting the radar to detect targets on top of a distance corresponding to the time delay. As a result, both factors, i.e., the unambiguous and maximum detection range, can be further extended, thus not limiting the system for practical applications.

The demonstrated system is also promising to be developed with a small form factor. The reflection of fiber Bragg grating combined with an optical circulator can form a bandpass filter with a compact size to replace the benchtop optical filter for ASE noise suppression. The synthesized bandwidth can be controlled by simply turning on-off of the RF driving signal of the AOM to determine the round-trip times. The benchtop EDFA can be replaced with a compact EDFA (such as ACL-PM-mini-EDFA-24) that can offer sufficient gain to offset the in-loop losses. On-chip components, such as AOM [48], [49], bandpass filter [50], and waveguide amplifier [51], are also promising to reduce the optical system's size further. A commercial data acquisition (DAQ) unit could be sufficient to simultaneously generate the RF driving signal and acquire the demodulated signal, therefore minimizing the system's electronic footprint. Such a device could be used in many resolution-demanding scenarios, such as hand gesture control [52], [53] and fall detection [54].

IV. Conclusion

In conclusion, we demonstrated a photonic SF waveform generation with a tunable bandwidth of $>$30 GHz and MHz-level frequency steps for high-resolution radar detections. By stabilizing polarization and reducing inter-pulse interference in the optical FSL, we significantly improve the SNR of the SF signals from 17 dB to 34 dB, allowing for imaging performance comparable to those using high-speed apparatus. The demonstrated system can provide a viable approach to overcome the analog bandwidth of digital waveform generators for synthesizing broadband radar signals, enabling high-resolution radar sensing and representing an attractive combination of wideband signal synthesizing, high SNR, and reduced hardware requirements. This work serves as a pilot study and experimental basis for future ultra-high-resolution, miniaturized, and mobile millimeter-wave devices with prime performance and flexibility.

References

[1] I. Duling and D. Zimdars, "Terahertz imaging: Revealing hidden defects," *Nature Photon.*, vol. 3, no. 11, pp. 630–632, 2009.

[2] H. W. Hübers, "Terahertz technology: Towards THz integrated photonics," *Nature Photon.*, vol. 4, no. 8, pp. 503–504, 2010.

[3] A. A. Gowen, C. O'Sullivan, and C. P. O'Donnell, "Terahertz time domain spectroscopy and imaging: Emerging techniques for food process monitoring and quality control," *Trends Food Sci. Technol.*, vol. 25, no. 1, pp. 40–46, 2012.

[4] M. Caruso, M. Bassi, A. Bevilacqua, and A. Neviani, "A 2–16 GHz 65 nm CMOS stepped-frequency radar transmitter with harmonic rejection for high-resolution medical imaging applications," *IEEE Trans. Circuits Syst. I: Regular Papers*, vol. 62, no. 2, pp. 413–422, Feb. 2015.

[5] K. Sengupta, T. Nagatsuma, and D. M. Mittleman, "Terahertz integrated electronic and hybrid electronic-photonic systems," *Nature Electron.*, vol. 1, no. 12, pp. 622–635, 2018. [Online]. Available: http://dx.doi.org/10.1038/s41928-018-0173-2

[6] S. Tonda-Goldstein, D. Dolfi, A. Monsterleet, S. Formont, J. Chazelas, and J. P. Huignard, "Optical signal processing in radar systems," *IEEE Trans. Microw. Theory Techn.*, vol. 54, no. 2, pp. 847–853, Feb. 2006.

[7] G. Serafino, S. Maresca, C. Porzi, F. Scotti, P. Ghelfi, and A. Bogoni, "Microwave photonics for remote sensing: From basic concepts to high-level functionalities," *J. Lightw. Technol.*, vol. 38, no. 19, pp. 5339–5355, 2020.

[8] P. Ghelfi *et al.*, "A fully photonics-based coherent radar system," *Nature*, vol. 507, no. 7492, pp. 341–345, 2014.

[9] B. Li, W. Wei, D. Han, W. Xie, and Y. Dong, "Remote broadband RF signal down-conversion with stable phase and high efficiency using a sideband optical phase-locked loop," *Opt. Exp.*, vol. 28, no. 9, pp. 12588–12598, 2020.

[10] E. A. Kittlaus *et al.*, "A low-noise photonic heterodyne synthesizer and its application to millimeter-wave radar," *Nature Commun.*, vol. 12, no. 1, pp. 1–10, 2021. [Online]. Available: http://dx.doi.org/10.1038/s41467-021-24637-0

[11] F. Falconi, C. Porzi, A. Malacarne, F. Scotti, P. Ghelfi, and A. Bogoni, "UWB FastlyTunable 0.5–50 GHz RF transmitter based on integrated photonics," *J. Lightw. Technol.*, vol. 40, no. 6, pp. 1726–1734, 2022.

[12] C. Porzi, F. Falconi, M. Sorel, P. Ghelfi, and A. Bogoni, "Flexible millimeter-wave carrier generation up to the sub-THz with silicon photonics filters," *J. Lightw. Technol.*, vol. 39, no. 24, pp. 7689–7697, Dec. 2021.

[13] X. Ye, F. Zhang, Y. Yang, and S. Pan, "Photonics-based radar with balanced I/Q de-chirping for interference-suppressed high-resolution detection and imaging," *Photon. Res.*, vol. 7, no. 3, pp. 265–272, 2019.

[14] G. Serafino *et al.*, "Toward a new generation of radar systems based on microwave photonic technologies," *J. Lightw. Technol.*, vol. 37, no. 2, pp. 643–650, Jan. 2019.

[15] G. Han, S. Li, X. Xue, and X. Zheng, "Photonic fractional Fourier transformer for chirp radar with ghost target elimination," *Opt. Lett.*, vol. 45, no. 15, pp. 4228–4231, 2020.

[16] S. Pan and J. Yao, "Photonics-based broadband microwave measurement," *J. Lightw. Technol.*, vol. 35, no. 16, pp. 3498–3513, 2017.

[17] J. Tang *et al.*, "Integrated optoelectronic oscillator," *Opt. Exp.*, vol. 26, no. 9, pp. 554–557, 2018.

[18] D. Marpaung, J. Yao, and J. Capmany, "Integrated microwave photonics," *Nature Photon.*, vol. 13, no. 2, pp. 80–90, 2019.

[19] T. Hao *et al.*, "Recent advances in optoelectronic oscillators," *Adv. Photon.*, vol. 2, no. 4, 2020, Art. no. 044001.

[20] Z. Ge, T. Hao, J. Capmany, W. Li, N. Zhu, and M. Li, "Broadband random optoelectronic oscillator," *Nature Commun.*, vol. 11, no. 1, pp. 1–8, 2020.

[21] T. Tetsumoto, T. Nagatsuma, M. E. Fermann, G. Navickaite, M. Geiselmann, and A. Rolland, "Optically referenced 300 GHz millimetre-wave oscillator," *Nature Photon.*, vol. 15, no. 7, pp. 516–522, 2021. [Online]. Available: http://dx.doi.org/10.1038/s41566-021-00790-2

[22] H. Chi, C. Wang, and J. Yao, "Photonic generation of wideband chirped microwave waveforms," *IEEE J. Microw.*, vol. 1, no. 3, pp. 787–803, Jul. 2021.

[23] A. Rashidinejad, Y. Li, J. M. Wun, D. E. Leaird, J. W. Shi, and A. M. Weiner, "Photonic generation and wireless transmission of W-band arbitrary waveforms with high time-bandwidth products," in *Proc. Conf. Lasers Electro-Opt. - Laser Sci. Photon. Appl.*, 2014 pp. 1–2.

[24] W. Liu *et al.*, "A fully reconfigurable photonic integrated signal processor," *Nature Photon.*, vol. 10, no. 3, pp. 190–195, 2016.

[25] S. Peng *et al.*, "High-resolution W-band ISAR imaging system utilizing a logic-operation-based photonic digital-to-analog converter," *Opt. Exp.*, vol. 26, no. 2, pp. 1978–1987, 2018.

[26] T. Hao *et al.*, "Breaking the limitation of mode building time in an optoelectronic oscillator," *Nature Commun.*, vol. 9, no. 1, pp. 1–8, 2018.

[27] R. Cheng, W. Wei, W. Xie, and Y. Dong, "Photonic generation of programmable coherent linear frequency modulated signal and its application in X-band radar system," *Opt. Exp.*, vol. 27, no. 26, pp. 37469–37480, 2019.

[28] S. Pan and Y. Zhang, "Microwave photonic radars," *J. Lightw. Technol.*, vol. 38, no. 19, pp. 5450–5484, 2020.

[29] X. Zhang, H. Zeng, J. Yang, Z. Yin, Q. Sun, and W. Li, "Novel RF-source-free reconfigurable microwave photonic radar," *Opt. Exp.*, vol. 28, no. 9, pp. 13650–13661, 2020.

[30] W. Xie *et al.*, "Optical linear frequency sweep based on a mode-spacing swept comb and multi-loop phase-locking for FMCW interferometry," *Opt. Exp.*, vol. 29, no. 2, pp. 604–614, 2021.

[31] Y. Fu, X. Zhang, B. Hraimel, T. Liu, and D. Shen, "Mach-Zehnder: A review of bias control techniques for Mach-Zehnder modulators in photonic analog links," *IEEE Microw. Mag.*, vol. 14, no. 7, pp. 102–107, Nov./Dec. 2013.

[32] J. Zhang and J. Yao, "Time-stretched sampling of a fast microwave waveform based on the repetitive use of a linearly chirped fiber Bragg grating in a dispersive loop," *Optica*, vol. 1, no. 2, pp. 64–69, 2014.

[33] P. Zhou, F. Zhang, Q. Guo, and S. Pan, "Linearly chirped microwave waveform generation with large time-bandwidth product by optically injected semiconductor laser," *Opt. Exp.*, vol. 24, no. 16, pp. 18460–18467, 2016.

[34] P. Zhou, R. Zhang, N. Li, Z. Jiang, and S. Pan, "An RF-source-free reconfigurable microwave photonic radar with high-resolution and fast detection capability," *J. Lightw. Technol.*, vol. 8724, pp. 1–1, 2022.

[35] C. Nguyen and J. Park, *Stepped-Frequency Radar Sensor Analysis*. New York, NY, USA: Springer, 2016.

[36] C. Schnébelin, J. Azaña, and H. Guillet de Chatellus, "Programmable broadband optical field spectral shaping with megahertz resolution using a simple frequency shifting loop," *Nature Commun.*, vol. 10, no. 1, pp. 1–11, 2019.

[37] Z. Zhang, Y. Liu, M. Burla, and B. J. Eggleton, "5.6-GHz-Bandwidth photonic stepped-frequency radar using MHz-level frequency-shifting modulation," in *Proc. Conf. Lasers Electro-Opt.*, 2020, pp. 1–2.

[38] Y. Zhang *et al.*, "Multi-functional radar waveform generation based on optical frequency-time stitching method," *J. Lightw. Technol.*, vol. 39, no. 2, pp. 458–464, 2021.

[39] Y. Liu, Z. Zhang, M. Burla, and B. J. Eggleton, "11-GHz-bandwidth photonic radar using MHz electronics," *Laser Photon. Rev.*, vol. 16, no. 4, Apr. 2022, Art. no. 2100549..

[40] Y. Lyu, Y. Li, C. Yu, L. Yi, T. Nagatsuma, and Z. Zheng, "Photonic generation of highly-linear ultra-wideband stepped-frequency microwave signals with up to 6.10^6 time-bandwidth product," *J. Lightw. Technol.*, vol. 40, no. 4, pp. 1036–1042, 2022.

[41] H. G. De Chatellus, L. Romero Cortés, C. Schnébelin, M. Burla, and J. Azaña, "Reconfigurable photonic generation of broadband chirped waveforms using a single CW laser and low-frequency electronics," *Nature Commun.*, vol. 9, no. 1, pp. 1–12, 2018.

[42] L. Zhang *et al.*, "Resolution enhancement for inversed synthetic aperture radar imaging under low SNR via improved compressive sensing," *IEEE Trans. Geosci. Remote Sens.*, vol. 48, no. 10, pp. 3824–3838, Oct. 2010.

[43] C. Ozdemir, *Inverse Synthetic Aperture Radar Imaging With MATLAB Algorithms*. Hoboken, NJ, USA: Wiley, 2012. [Online]. Available: http://ebookcentral.proquest.com/lib/usyd/detail.action?docID=818515

[44] N. Levanon, "Stepped-frequency pulse-train radar signal," *IEE Proc. Radar, Sonar and Navigation*, vol. 149, no. 6, pp. 297–309, 2002.

[45] V. Billault *et al.*, "Coherent optical fiber sensing based on a frequency shifting loop," *J. Lightw. Technol.*, vol. 39, no. 12, pp. 4118–4123, Jun. 2021.

[46] A. Gustavsson, P. Frklind, H. Hellsten, T. Jonsson, B. Larsson, and G. Stenstrom, "The airborne VHF SAR system CARABAS," in *Proc. IEEE/IGARSS'93 Int. Geosci. Remote Sens. Symp.*, 1990, pp. 558–562,.

[47] S. Pinna *et al.*, "Photonics-based radar for sub-mm displacement sensing," *IEEE J. Sel. Topics Quantum Electron.*, vol. 23, no. 2, pp. 168–175, Mar./Apr. 2017.

[48] L. Shao *et al.*, "Integrated lithium niobate acousto-optic frequency shifter," in *Opt. InfoBase Conf. Papers*, vol. Part F183-, no. 16, pp. 23728–23738, 2020.

[49] Z. Yu and X. Sun, "Gigahertz acousto-optic modulation and frequency shifting on etchless lithium niobate integrated platform," *ACS Photon.*, vol. 8, no. 3, pp. 798–803, 2021.

[50] K. Wang, Y. Wang, X. Guo, Y. Zhang, A. He, and Y. Su, "Ultracompact bandwidth-tunable filter based on subwavelength grating-assisted contra-directional couplers," *Front. Optoelectron.*, vol. 14, no. 3, pp. 374–380, Sep. 2021. [Online]. Available: https://link.springer.com/10.1007/s12200-020-1056-5

[51] C. Vagionas *et al.*, "Lossless 1×4 silicon photonic ROADM based on a monolithic integrated erbium doped waveguide amplifier on a Si_3N_4 platform," *J. Lightw. Technol.*, vol. 40, no. 6, pp. 1718–1725, Mar. 2022. [Online]. Available: https://ieeexplore.ieee.org/document/9627806/

[52] Z. Zhang, Z. Tian, and M. Zhou, "Latern: Dynamic continuous hand gesture recognition using FMCW radar sensor," *IEEE Sensors J.*, vol. 18, no. 8, pp. 3278–3289, Apr. 2018.

[53] J. Park, J. Jang, G. Lee, H. Koh, C. Kim, and T. W. Kim, "A time domain artificial intelligence radar system using 33-GHz direct sampling for hand gesture recognition," *IEEE J. Solid-State Circuits*, vol. 55, no. 4, pp. 879–888, Apr. 2020.

[54] M. G. Amin, Y. D. Zhang, F. Ahmad, and K. C. Ho, "Radar signal processing for elderly fall detection: The future for in-home monitoring," *IEEE Signal Process. Mag.*, vol. 33, no. 2, pp. 71–80, Mar. 2016.

Ziqian Zhang received the bachelor's degree in underwater acoustic engineering from Harbin Engineering University, Harbin, China, in 2015, and the master's degree (Ph.M.) in telecommunications engineering in 2018 from The University of Sydney, Sydney, NSW, Australia, where he is currently working toward the Ph.D. degree in physics. His research interests include integrated microwave photonics, photonic radar, and LiDAR.

Yang Liu received the bachelor's degree in optoelectronics from the Huazhong University of Science and Technology (HUST), Wuhan, China, in 2012, the master's degree in optical engineering from the Wuhan National Laboratory for Optoelectronics (WNLO) and HUST, in 2015, and the Ph.D. degree in physics with Nonlinear Photonics Group, Centre for Ultrahigh Bandwidth Devices for Optical Systems, School of Physics, The University of Sydney, Sydney, NSW, Australia, in 2019. He was a Postdoctoral Research Associate leading integrated microwave photonics and hybrid integration research activities with The University of Sydney. He joined the Laboratory of Photonics and Quantum Measurements, EPFL, Lausanne, Switzerland, as a Postdoctoral Researcher in December 2020, holding a Marie Skłodowska-Curie Individual Fellowship. His research interests include the fundamentals and applications of nonlinear optics, integrated microwave photonics, photonic radars, and frequency microcombs. He was the recipient of the Chinese Government Award for Distinguished Self-financed Student Abroad in 2019.

Benjamin J. Eggleton (Fellow, IEEE) received the bachelor's (Hons.) degree in science and the Ph.D. degree in physics from The University of Sydney, Sydney, NSW, Australia, in 1992 and 1996, respectively. In 1996, he joined Bell Laboratories, Lucent Technologies, Murray Hill, NJ, USA, as a Postdoctoral Member of Staff, and then transferred to the Department of Optical Fiber Research. In 2000, he became the Research Director within the Specialty Fiber Business Division, Lucent Technologies. He is currently a Professor in physics with The University of Sydney, the Director of The University of Sydney Nano Institute, Sydney, NSW, Australia, and the Co-Director of the NSW Smart Sensing Network (NSSN). He was the Director of the ARC Centre of Excellence for Ultrahigh Bandwidth Devices for Optical Systems (CUDOS). He is the author or coauthor of more than 500 journal publications. His research interests include nonlinear optics, all-optical signal processing, optical communications, photonic crystals, and stimulated Brillouin scattering. He is a Fellow of the Australian Academy of Science, Australian Academy of Technology and Engineering, and Optical Society of America. He was the recipient of the 2020 WH Beattie Steel Medal from the Australian and New Zealand Optical Society, Pawsey Medal from the Australian Academy of Science, 2004 Malcolm McIntosh Prize for Physical Scientist of the Year, 2003 International Commission on Optics Prize, 1998 Adolph Lomb Medal from the Optical Society of America, Distinguished Lecturer Award from the IEEE/Lasers and Electro-Optics Society, and Research and Development 100 Award. He was the President of the Australian Optical Society during 2008–2010. He is currently an Editor-in-Chief of *APL Photonics*.